CHEMISTRY
A EUROPEAN JOURNAL

ChemPubSoc
Europe

DOI: 10.1002/chem.201200696

VIP

Tailor-Made Metal–Organic Frameworks from Functionalized Molecular Building Blocks and Length-Adjustable Organic Linkers by Stepwise Synthesis

Ya-Qian Lan,[a, b] Shun-Li Li,[b] Hai-Long Jiang,[a] and Qiang Xu*[a]

Abstract: In this work, we have demonstrated a family of diamondoid metal–organic frameworks (MOFs) based on functionalized molecular building blocks and length-adjustable organic linkers by using a stepwise synthesis strategy. We have successfully achieved not only "design" and "control" to synthesize MOFs, but also the functionalization of both secondary building units (SBUs) and organic linkers in the same MOF for the first time. Furthermore, the results of N_2 and H_2 adsorption show that their surface areas and hydrogen uptake capacities are determined by the most optimal combination of functional groups from SBUs and organic linkers, interpenetration, and free volume in this system. A member of this series, **DMOF-6** exhibits the highest surface area and H_2 adsorption capacity among this family of MOFs.

Keywords: adsorption · building blocks · metal–organic frameworks · synthetic methods

Introduction

Metal–organic frameworks (MOFs) have been the focus of great interest due to not only their structural and chemical diversities but also the potential structure-related applications, such as luminescence, gas storage, catalysis, separations, and drug delivery.[1,2] In general, MOFs are assembled in "one-pot" solvothermal syntheses in which topology control is accomplished only by careful selection of the metal, organic linker, and synthetic conditions.[3] Great successes have been obtained through this simple synthetic route, which is, however, limited for targeted syntheses and often uncontrollable. One of the most important goals in the synthesis of MOFs is to achieve "design" and "control" to obtain tailor-made compounds with expected structures and properties starting from well-characterized inorganic and organic precursors.[4] A stepwise synthesis strategy undoubtedly may help to shed light on this goal and lead to multifunctional MOFs with special characteristics.

Recently, the molecular building block (MBB) approach has been a powerful strategy for the design and construction of MOFs.[5,6] The MBBs can act as secondary building units (SBUs),[7] which are theoretically connected by organic linkers or metal cations to construct multifunctional MOFs from predesigned MBBs by using a stepwise synthesis strategy. However, it is largely limited in the construction of MOFs due to the difficulties of selecting MBBs and the restriction of solvothermal synthesis conditions. Hitherto, only a few MOFs have been observed using this synthesis strategy by the groups of Zhou, Zaworotko, and Su.[8] They have successfully demonstrated some examples from 0D metal–organic polyhedra (MOP) to 3D MOFs by using predesigned MBBs, in which the MOPs (tetrahedron,[8a] octahedron,[8b] trigonal prism,[8c] and cuboctahedron[8d]) act as supramolecular building blocks.

On the other hand, the functionalization of MOFs has attracted ever increasing scientific interest for expanding the chemical diversity and potential applications. The postsynthetic modification (PSM) approach has made great achievements in the functionalization of MOFs.[9–11] The most common is covalent PSM of the organic linkers within the MOFs. Some discussion of dative PSM is the modification of unsaturated metal sites located at the SBUs of MOFs through a dative (i.e., metal–ligand) bond.[9e] However, there is an unfavorable lack of investigation on the functionalization of both the organic linker and SBU in the same MOFs. Moreover, the functional MOFs of PSM often display poorer crystallinity and single-crystal data cannot be obtained upon PSM process, which means that the accurate structures cannot be determined. To overcome these difficulties, it is necessary to introduce a new synthetic strategy. If we can synthesize functionalized MBBs and combine them with some ligands that are modified by functional groups and alterable lengths, we will successfully achieve the functionalization of MOFs that consist of both the functionalized MBBs and length-adjustable and functional or-

[a] Dr. Y.-Q. Lan, Dr. H.-L. Jiang, Prof. Dr. Q. Xu
National Institute of Advanced Industrial Science and Technology (AIST)
Ikeda, Osaka 563-8577 (Japan)
E-mail: q.xu@aist.go.jp

[b] Dr. Y.-Q. Lan, Dr. S.-L. Li
Faculty of Chemistry
Northeast Normal University
Changchun 130024 (P. R. China)

Supporting information for this article, including PXRD, TG curves of compounds, additional figures and gas sorption isotherms, is available on the WWW under http://dx.doi.org/10.1002/chem.201200696.

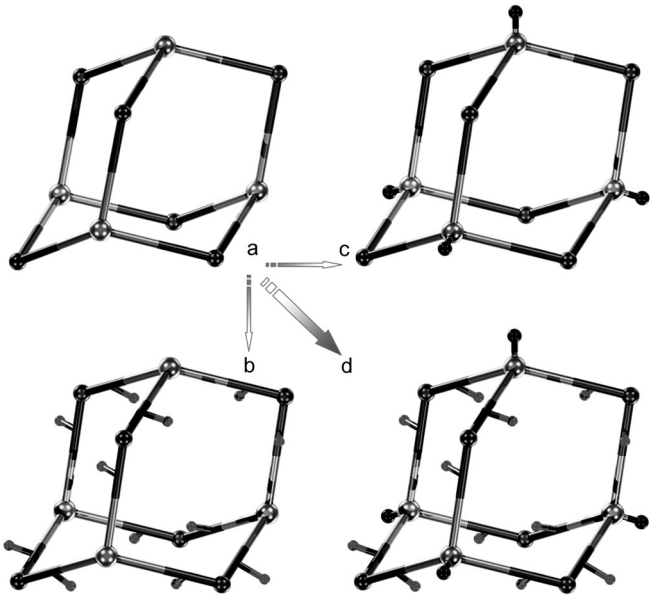

Scheme 1. Schematic illustration for functionalization of MOFs: a) the general MOF, b) covalent PSM of the organic linkers, c) the modification of unsaturated metal sites located at the SBUs of MOFs, and d) functionalization of both SBUs and organic linkers.

ganic linkers in crystallinity system without using PSM (Scheme 1). To date, there have been no reports using this kind of system.

As shown above, we are looking for an ideal system of a stepwise synthesis of MOFs that can achieve not only design and control but also the functionalization of both SBUs and length-adjustable organic ligands while keeping the same framework topology. The four-connected diamondoid network plays an important role in MOFs.[12] Metal–organic materials first appeared on the scene when it was realized that the geometric features of tetrahedral cations could be used to design four-connected diamondoid networks[10] by simply bonding the metal cations to linear bifunctional organic ligands. We will use the predesigned tetrahedral MBB (TMBB) and a series of tetratopic ligands with functional groups and adjustable lengths to obtain the functionalization of a diamondoid MOFs system by using a stepwise synthesis strategy under solvothermal conditions. After careful consideration, we chose the nanoscale pentanuclear metal clusters $[Zn_5(btz)_6(NO_3)_4(H_2O)]$ (**TMBB-1**), $[Zn_5(dme\text{-}btz)_6Cl_4(H_2O)_2]$ (**TMBB-2**), and $[Zn_5(me\text{-}btz)_6Cl_4(H_2O)_2]$ (**TMBB-3**) (btz = benzotriazole, dme-btz = 5,6-dimethylbenzotriazole, me-btz = 5-methylbenzotriazole, Figure 1 and Scheme S8 in the Supporting Information) as initial reaction precursors. We also deliberately designed a series of tetratopic ligands with functional groups and adjustable lengths (namely, H_4L^1, H_4L^2, H_4L^3, H_4L^4, H_4L^5, and H_4L^6, Figure 1 and Scheme S9 in the Supporting Information) as organic linkers. These precursors and ligands were chosen based on the following considerations: 1) The tetrahedral MBBs can be modified by changing the functional groups of btz to readily obtain functionalized MBBs. 2) The MBBs have the advantage of being readily soluble in some organic solvents while retaining their original structures according to previous literature,[4,8a] to ensure the feasibility of the subsequent cluster framework formation. 3) The tetratopic ligands with functional groups and adjustable length show tetrahedral coordination geometry, which facilitates the formation of a diamondoid network and functionalization of MOFs.

Fortunately, we have obtained a family of microporous diamondoid MOFs (**DMOF-*n***, $n = 1$–15) (Tables S1 and S2 in the Supporting Information) based on single-crystal X-ray structural and PXRD data, which are in agreement with our prior expectations. To the best of our knowledge, these are the first examples of MOFs based on functionalized MBBs and length-extendable and functional organic linkers by a stepwise synthesis strategy. Moreover, with the increase of the length of the organic linker, the degrees of interpenetration have been regulated in the diamondoid topological MOFs system. The results of N_2 and H_2 gas adsorption show that their surface areas and hydrogen uptake capacities are not linear, but are determined by the most optimal combination of functional groups, interpenetration, and free volume in this system.

Results and Discussion

Single-crystal X-ray analysis revealed that **TMBB-1** or **2** consists of five Zn cations and six deprotonated btz ligands or their derivatives. The pentanuclear metal cluster shows a tetrahedral structure, in which four Zn^{2+} ions are located at each vertex of the tetrahedron and the fifth Zn^{2+} ion inlays the center with distorted octahedral coordination geometry. Each Zn^{2+} ion at the apical positions bears a chelating nitrate or Cl^- group (Figure 1 and Figure S1 in the Supporting Information). Comparison of the experimental PXRD pattern of as-synthesized **TMBB-3** with the simulated diffraction pattern of **TMBB-2**, the very high degree of correspondence between the patterns indicates that the bulk material has the same structure as **TMBB-2** (Figure S23 in the Supporting Information).

Isostructural $[Zn_5(btz)_6(L^1)(H_2O)]$ (**DMOF-1**), $[Zn_5(bm\text{-}btz)_6(L^1)(H_2O)]$ (**DMOF-2**) and $[Zn_5(m\text{-}btz)_6(L^1)(H_2O)]$ (**DMOF-3**) have been obtained based on **TMBB-*n*** and tetratopic ligand H_4L^1 in DMF. **DMOF-1** and **DMOF-2** crystallize in the monoclinic space group $C2/c$ and **DMOF-3** crystallizes in the triclinic space group $P\bar{1}$. As expected, all nitrate or Cl^- groups that were bonded to the apical sites of **TMBB-*n*** were replaced by $(L^1)^{4-}$. The asymmetric unit contains one pentanuclear metal cluster (named SBU-*n*), which is **TMBB-*n*** losing anions, one deprotonated $(L^1)^{4-}$ ligand and one coordinated water molecule. Each SBU is connected by four carboxylate ligands $(L^1)^{4-}$ to be a 4-connected node, and each $(L^1)^{4-}$ connects four SBUs, for which each carboxylic group binds to one SBU. Such connectivity leads to a highly porous extended 3D framework with a typically **dia** network. Further study into the nature of this architec-

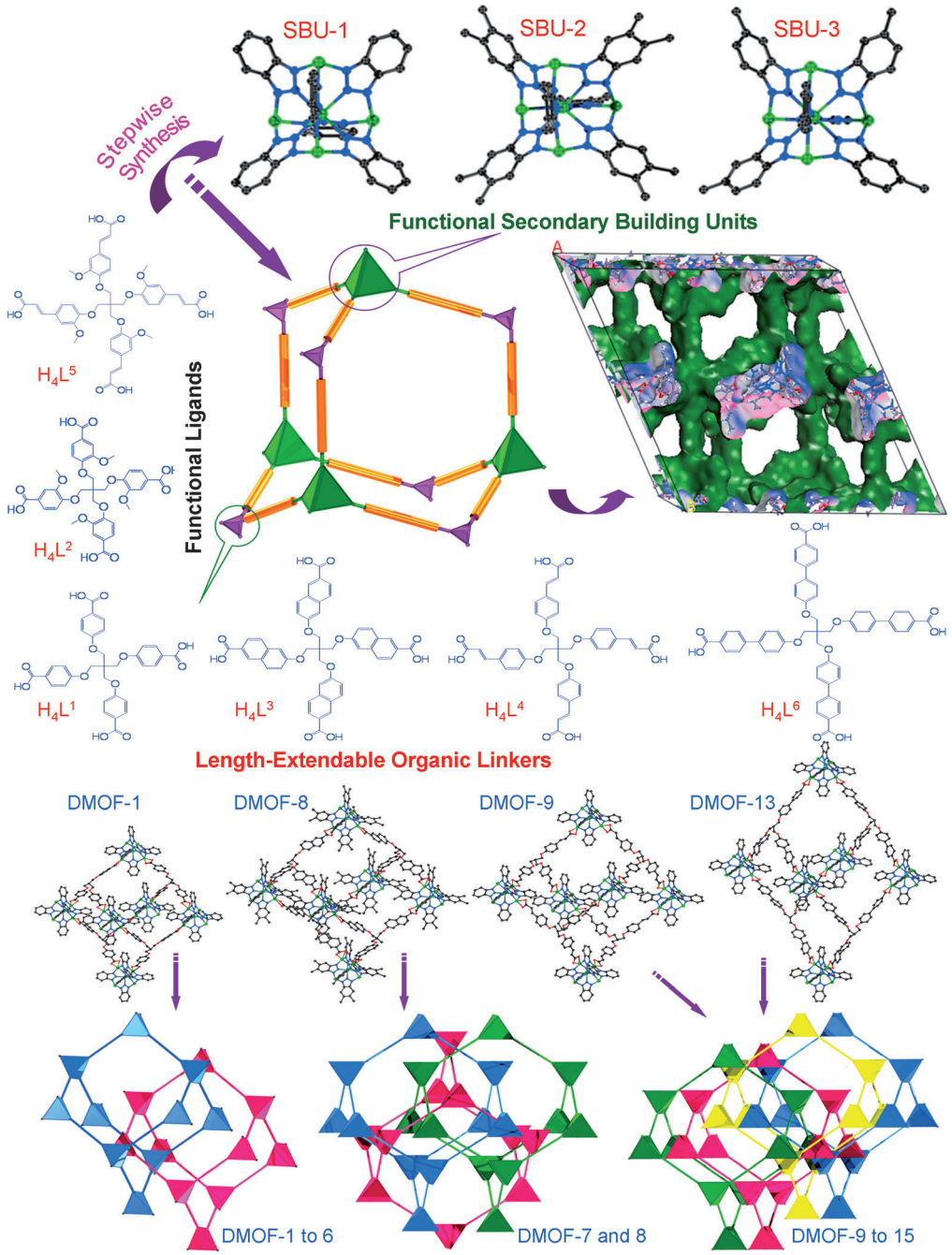

Figure 1. Stepwise synthesis of MOFs based on functionalized MBBs and length-adjustable organic linkers with functional groups, the single adamantanoid cages in **DMOF-1**, **DMOF-8**, **DMOF-9**, and **DMOF-13**, and the twofold, threefold, and fourfold interpenetration topology in **DMOF-1** to **6**, **DMOF-7** and **8**, and **DMOF-9** to **15**, respectively.

ture reveals that two types of cages arrange alternately to form the single network, one is comprised of six SBUs and four L^1 ligands, and the other contains four SBUs and six L^1 ligands The spacious nature of the single network allows other identical **dia** networks to penetrate it in a normal mode,[13] thus resulting in twofold interpenetrating **dia** arrays (Figure 1 and Figures S2–S5 in the Supporting Information).

The above-mentioned results encouraged us to expand our studies to construct targeted networks based on functional and length-extendable organic linkers. When using longer H_4L^4 and H_4L^6 tetratopic ligands instead of the H_4L^1 ligand, for which the corresponding length increases from 8.5 to 10.6 and 12.7 Å, respectively (the distance is between the central C atom and the O atom of carboxyl group, Scheme S9 in the Supporting Information), **DMOF-9** to **11** and **DMOF-13** to **15** with the same framework topology were obtained. As noted previously for **DMOF-1**, **DMOF-9**, **DMOF-11**, and **DMOF-13** all crystallize in the monoclinic space group *C*2/*c*. As anticipated, their structures are com-

posed of pentanuclear zinc clusters with different btz ligands (or its derivatives) that are joined through long deprotonated $(L^4)^{4-}$ and $(L^6)^{4-}$ ligands, and again consist of similar **dia** frameworks. With the increase in the length of the organic ligands, the longest dimensions of cages change largely from 35.036 (**DMOF-1**) to 38.016 (**DMOF-9**) and 50.348 Å (**DMOF-13**) (Figure 1 and Figures S6–8 and S21 in the Supporting Information). Four such independent networks interpenetrate to generate a fourfold interpenetrating **dia** framework architecture in **DMOF-9**, **DMOF-11**, and **DMOF-13** (Figure S5 in the Supporting Information), which is consistent with the suggestion by Champness, Schöder, and coworkers that the longer ligands lead to a greater degree of interpenetration in the same topology.[14] The PXRD data of **DMOF-10** and **DMOF-14/15** are in good agreement with **DMOF-9** and **DMOF-13**, respectively, which demonstrates that **DMOF-10**, **DMOF-14**, and **DMOF-15** have the similar fourfold interpenetrating **dia** framework as **DMOF-9** and **DMOF-13** except the different functional groups of btz (Figure S24 in the Supporting Information).

When using the similar ligand H_4L^3 with a naphthyl group instead of H_4L^4, **DMOF-7** and **DMOF-8** $[Zn_{15}(bme\text{-}btz)_{18}(L^3)_3(H_2O)_2]$ (**DMOF-8**) were isolated based on **TMBB-1** and **TMBB-2. DMOF-8** crystallizes in the chiral space group *C*2. The asymmetric unit contains 3/2 pentanuclear metal clusters, 3/2 deprotonated $(L^3)^{4-}$ ligands and two coordinated water molecules (Figure 1 and Figures S9 and S10 in the Supporting Information). The longest dimension between the centers of the two pentanuclear zinc clusters is 38.685 Å in the **dia** cages, which is similar to **DMOF-9** (38.016 Å) (Figure S21 in the Supporting Information). It is interesting that **DMOF-8** is a threefold interpenetrating **dia** network, which is different from the fourfold interpenetration in **DMOF-9** and **DMOF-11**. The reason may be due to the larger steric hindrance from the naphthyl group of H_4L^3 than in H_4L^4, which is appropriate for the critical condition of interpenetrating change (Figure S5 in the Supporting Information). The experimental PXRD pattern of as-synthesized **DMOF-7** matches the simulated **DMOF-8** powder diffraction pattern, indicating that the microcrystal of **DMOF-7** has the same topological structure as **DMOF-8** (Figure S24 in the Supporting Information).

The organic linkers H_4L^2 and H_4L^5 with functional methoxy groups[15] were used to synthesize functionalized MOFs. $[Zn_5(btz)_6(L^2)(H_2O)_2]$ (**DMOF-4**), $[Zn_5(dme\text{-}btz)_6(L^2)]$ (**DMOF-5**), $[Zn_5(me\text{-}btz)_6(L^2)]$ (**DMOF-6**), and **DMOF-12** were successfully obtained based on different TMBBs in the similar solvothermal synthesis conditions as for **DMOF-1**. Similar to **DMOF-1**, isostructural **DMOF-4** to **6** all crystallize in the monoclinic space group *C*2/*c* and also have twofold interpenetrating **dia** frameworks (Figure 1 and Figure S5 in the Supporting Information). However, the unit-cell parameters of **DMOF-4** are different from those of **DMOF-1**; the asymmetric unit of **DMOF-4** contains half of a pentanuclear metal cluster (SBU-1), half of a deprotonated $(L^2)^{4-}$ ligand and one coordinated water molecule. The asymmetric units of **DMOF-5/6** are similar to **DMOF-2/3** except with $(L^2)^{4-}$ instead of $(L^1)^{4-}$ and the absence of coordinated water molecules (Figure 1 and Figures S11–13 and S21 in the Supporting Information). Most importantly, **DMOF-5** and **6** have been successfully synthesized with the functionalization of both SBUs and organic linkers in one crystalline framework. The successful isolation of these compounds demonstrates a rational strategy for functionalization of MOFs, with which we can carefully select and effectively combine different functional groups from SBUs and organic linkers to synthesize targeted functionalized MOFs. The PXRD data of **DMOF-12** are in good agreement with **DMOF-9**, which demonstrates that **DMOF-12** has a similar fourfold interpenetrating **dia** framework as **DMOF-9** except for the functional methoxy groups (Figure S24 in the Supporting Information).

The family of microporous **DMOF-*n*** was successfully achieved, which proves that we can design and control this system by using a stepwise synthesis strategy. To further confirm our viewpoint, as a representative of this system, we used btz ligands and Zn^{2+} ions as raw materials instead of **TMBB-1** to synthesize **DMOF-1** with the same stoichiometry by using a one-pot reaction method. We obtained two compounds: one was a small amount of **DMOF-1**, and the other was 4,6-connected self-penetrating topological **MOF-01**. The asymmetric unit of **MOF-01** contains three deprotonated btz ligands, four Zn atoms and 3/2 deprotonated $(L^1)^{4-}$ ligands. Compared with **DMOF-1**, the SBU of **MOF-01** consists of three deprotonated btz ligands and four Zn atoms, which is different from the tetrahedral SBU-1 in **DMOF-1** that contains six deprotonated btz ligands and five Zn atoms (Figures S14–16 in the Supporting Information). These experimental results indicate that the stepwise synthetic routes using **TMBB** can be easily controlled to obtain the targeted MOFs whereas it is difficult or uncontrollable with the one-pot reaction method (Figure 2).

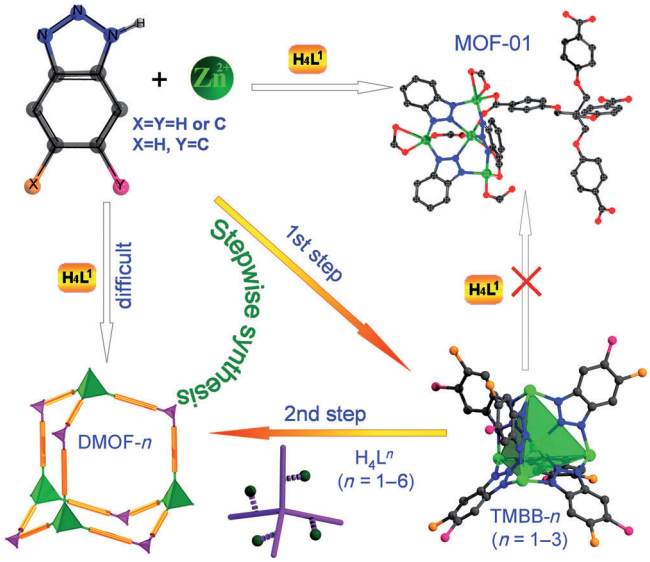

Figure 2. Stepwise and one-pot reaction methods for the synthesis of **DMOF-*n***.

The common nature of **DMOF-*n*** is that only two of the four hands from the tetratopic ligand link SBUs to form an infinite helical chain in one single diamondoid net. In twofold interpenetrating compounds **DMOF-1** to **6**, two infinite helical chains from two individual diamondoid nets with the same chirality entangle each other to form a double helical unit (Figure S17 in the Supporting Information). In threefold interpenetrating **DMOF-8**, three infinite helical chains from individual diamondoid nets show the same chirality and one chain enwinds simultaneously the other two helical chains that are arranged in parallel without intertwinement to form a special triple-stranded helix, which is different from conventional triple-stranded helices and a molecular braid reported recently[15] (Figures S18–S20 in the Supporting Information). In **DMOF-9**, **DMOF-11**, and **DMOF-13**, four such helical chains from four individual **dia** nets are divided into two groups; each group is composed of a pair of non-intertwined helices of opposite helicity. Two groups of non-intertwined double helices are interwoven in such a way that the openings generated by one group of helices are alternately penetrated by two helices of the other group, thus resulting in an inextricable quadruple-stranded braid (Figures S19 and S20 in the Supporting Information). This peculiar entangled topology in MOFs was only reported recently.[8a]

Furthermore, compared with the size of the adamantanoid cage in **DMOF-*n***, we find that the degrees of interpenetration are dependent on the shortest distances of cages, which are less than 28.972 Å in **DMOF-1** to **6** showing a twofold interpenetrating **dia** framework, equal to 34.806 Å in **DMOF-8** with threefold interpenetration, and larger than 36.494 Å in **DMOF-9**, **11**, and **13** showing fourfold interpenetrating networks (Figures S5 and S21 in the Supporting Information). Despite the interpenetration, the frameworks of **DMOF-*n*** remain microporous and have free porosities that are occupied by crystallographically unresolved solvent molecules. The space-filling models of **DMOF-*n*** along the different directions exhibit those feature of microporous materials. **DMOF-1** has microporous channels (about 4×8 Å^2, the van der Waals radii are excluded) viewed along the *b* axes. The sizes of micropores are approximately 5×6 and $4\times4/8\times15$ Å^2 (the van der Waals radii are excluded) in threefold interpenetrating **DMOF-8** and fourfold interpenetrating **DMOF-11/13** viewed along the *c*-axis, respectively (Figure S22 in the Supporting Information). PLATON[17] analysis showed that the highest porosity is 66.4% in **DMOF-1** and the lowest is 49.2% in **DMOF-11**, owing to the influence of different functional groups and the degrees of interpenetration in **DMOF-*n*** (Table S3 in the Supporting Information).

The porosities of **DMOF-*n*** make their frameworks possible for use in gas storage, and provide us with the chance to study the influence of the functional groups of the MBBs and organic linkers, and interpenetration on gas storage. The N_2 sorption isotherms of **DMOF-*n*** at 77 K show characteristic type I behavior for microporous materials with a slight hysteresis between the adsorption and desorption, which can be explained by the dynamic feature and cage effect of the frameworks (Figure 3 and Figures S25–27 in the Supporting Information).[18] The H_2 uptake capacity of twofold interpenetrating **DMOF-1** to **6** is 1.06, 0.69, 0.88, 0.59, 0.84, and 1.28 wt% (77 K, 1 bar), respectively. The trend of H_2 uptake capacity is consistent with the change of their N_2 adsorption amounts and surface areas in **DMOF-1** to **6**. The H_2 adsorption capacity of **DMOF-5** (0.84 wt%) and **DMOF-6** (1.28 wt%) with functional methoxy groups is higher than **DMOF-2** (0.69 wt%) and **DMOF-3** (0.88 wt%) without methoxy groups, respectively. The N_2 adsorption amount of **DMOF-7** (142.7 cm^{3}g^{-1}) is higher than **DMOF-8** (110.5 cm^{3}g^{-1}) in the 3-fold interpenetrating framework, whereas it presents opposite results in the H_2 uptake capacity (**DMOF-8**, 1.02 wt% and **DMOF-7**, 0.84 wt%) (Figure S28 in the Supporting Information). It is assumed that methyl groups favor H_2 adsorption. The H_2 uptake capacity is 0.55, 0.48, 0.74, and 0.30 wt% in 4-fold interpenetrating **DMOF-9** to **12** based on the similar length of H_4L^4 and H_4L^5, respectively. Relative to their low BET surface areas (179, 43, 120, and 2 m^{2}g^{-1}), the H_2 adsorption capacity is gratifying, indicating that the catenation is beneficial to H_2 loading at low pressure.[19] The H_2 gas sorption isotherms for 4-fold interpenetrating **DMOF-13** to **15** reveal that the H_2 adsorption capacity of **15** (0.98 wt%) is higher than those of **13** (0.89 wt%) and **14** (0.76 wt%), which is consistent with the change of their surface areas. Among **DMOF-*n*, DMOF-6** with the functionalization of both SBUs and organic linkers exhibits the highest BET and Langmuir surface areas (971 and 1106 m^{2}g^{-1}), and H_2 adsorption amount (142.9 m^{3}g^{-1}, 1.28 wt%). For the **DMOFs** constructed from the organic linkers with the same length, the H_2 adsorption capacity of **DMOF** based on **TMBB-3** with one methyl group is higher than those based on **TMBB-1** and **TMBB-2** except for **DMOF-3**, which is lower than that of **DMOF-1**. From the N_2 and H_2 adsorption results, it is obvious that the surface areas and hydrogen uptake capacities are determined by the most optimal combination of functional groups from SBUs and organic linkers, interpenetration, and free volume in the system.[20] Bearing this in mind, we may carefully select and effectively combine functional groups of SBUs and organic linkers to improve hydrogen uptake (Figure 3and Table S3 and Figures S25–32 in the Supporting Information).

Conclusion

A family of microporous diamondoid MOFs was synthesized based on functionalized MBBs and length-extendable organic linkers with functional groups by using a stepwise synthesis strategy. As expected, we successfully achieved not only design and control to synthesize the MOFs but also the functionalization of both SBUs and organic linkers in the same MOFs for the first time. Moreover, with the increase in length of the organic linker, the degrees of interpenetration were regulated with the framework topology remaining

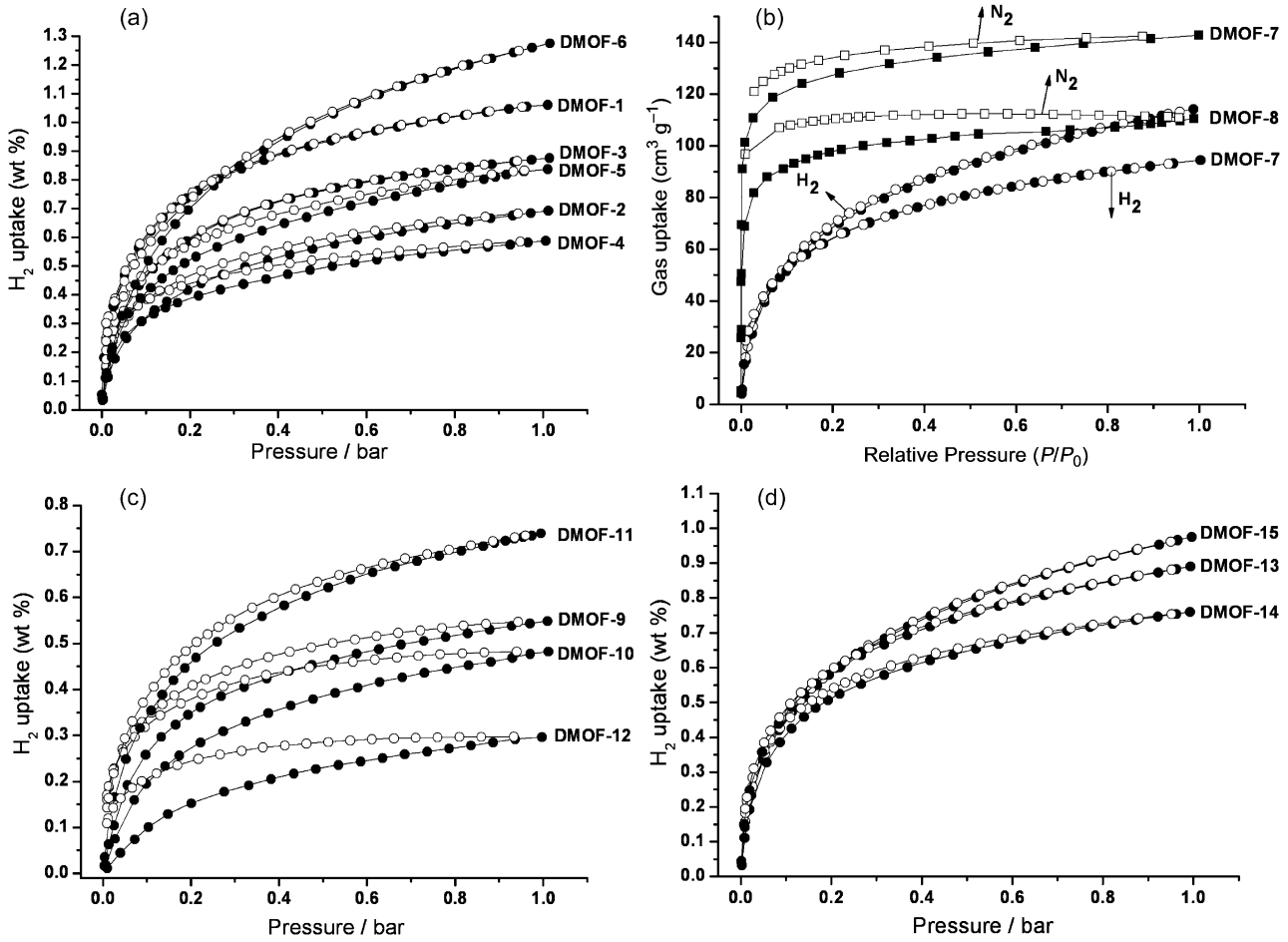

Figure 3. The gas sorption isotherms for **DMOF-*n*** at 77 K. a) The H_2 gas sorption isotherms for twofold interpenetrating **DMOF-1** to **6**. b) The N_2 and H_2 gas sorption isotherms for threefold interpenetrating **DMOF-7** and **8**. c) and d) The H_2 gas sorption isotherms for fourfold interpenetrating **DMOF-9** to **15**. The filled and open graphs represent adsorption and desorption branches, respectively.

unchanged. In addition, the results of N_2 and H_2 adsorption show that the surface areas and hydrogen uptake capacities are determined by the most optimal combination of functional groups, interpenetration, and free volume in the system. **DMOF-6** with the functionalization of both SBUs and ligands exhibits the highest surface area and H_2 adsorption capacity among this family of MOFs. With the stepwise synthesis strategy, as a general approach, rational choices of predesigned MBBs with different geometric polyhedra and functional organic linkers should lead to the discovery of abundant targeted porous materials with diverse characteristics in the near future.

Experimental Section

Synthesis of TMMB-1 [$Zn_5(btz)_6(NO_3)_4(H_2O)$]: A solution of [$Zn(NO_3)_2{\cdot}4H_2O$] (131 mg, 0.5 mmol) and benzotriazole (69 mg, 0.6 mmol) in methanol/DMA (1:1, 10 mL) was heated at 85 °C for 3 days in a Teflon-lined steel container. The resulting colorless crystals were collected, washed with Et_2O, and dried at room temperature (yield: 84.6 mg, 65 % based on Zn).

Synthesis of TMMB-2 [Zn_5(bme-btz)$_6Cl_4(H_2O)_2$]: A solution of $ZnCl_2$ (68 mg, 0.5 mmol) and 5,6-dimethylbenzotriazole hydrate (88 mg, 0.6 mmol) in methanol/DMA (1:2, 9 mL) was heated at 120 °C for 3 days in a Teflon-lined steel container. The resulting colorless crystals **TMBB-2** were collected, washed with Et_2O, and dried at room temperature (yield: 95 mg, 69 % based on Zn).

Synthesis of TMMB-3: A solution of $ZnCl_2$ (68 mg, 0.5 mmol) and 5-methylbenzotriazole (80 mg, 0.6 mmol) in methanol/DMA/H_2O (2:2:1, 10 mL) was heated at 120 °C for 3 days in a Teflon-lined steel bomb. The resulting colorless microcrystals were collected, washed with Et_2O, and dried at room temperature (yield: 74 mg, 57 % based on Zn).

Synthesis of DMOF-1 [$Zn_5(btz)_6(L^1)(H_2O)$]: A solid mixture of H_4L^1 (61.6 mg, 0.10 mmol) and **TMBB-1** (130.2 mg, 0.10 mmol) was dissolved in DMF (5 mL) in a 20 mL Teflon-lined stainless steel container. The clear reaction solution was heated in an isotherm oven at 85 °C for 72 h, resulting in colorless crystals that were isolated by washing with DMF (5 × 5 mL) and were immersed in dichloromethane for 24 h. After the removal of dichloromethane by decanting, the sample was dried under a dynamic vacuum at room temperature overnight. Yield: 125.0 mg, 75 % based on H_4L^1. IR (KBr): $\tilde{\nu}$ = 3447 (m), 2931 (m), 1672 (s), 1602 (s), 1504 (m), 1385 (s), 1303 (m), 1245 (s), 1171 (s), 1094 (s), 1057 (w), 1017 (w), 929 (w), 864 (w), 785 (s), 754 (m), 697 (w), 662 (m), 554 (w), 434 cm^{-1} (w).

Synthesis of MOF-01 [$Zn_8(L^1)_3(btz)_6$]: A solid mixture of H_4L^1 (61.6 mg, 0.10 mmol), [$Zn(NO_3)_2{\cdot}4H_2O$] (131 mg, 0.5 mmol) and benzotriazole (69 mg, 0.6 mmol) was dissolved in DMF (5 mL) in a 20 mL Teflon-lined

stainless steel container. The clear reaction solution was heated in an isotherm oven at 85 °C for 72 h, resulting in two kinds of colorless crystals, of which one is **DMOF-1** and the other is **MOF-01.**

Synthesis of DMOF-2 [Zn_5(bme-btz)$_6$(L^1)(H_2O)]: The same synthetic conditions as those used for the preparation of **DMOF-1** were used except with **TMBB-2** instead of **TMBB-1**. The colorless block crystals were isolated by washing with DMF and were immersed in dichloromethane for 24 h. After the removal of dichloromethane by decanting, the sample was dried under a dynamic vacuum at room temperature overnight. Yield: 106.4 mg, 58 % based on H_4L^1. IR (KBr): $\tilde{\nu}$ = 3859 (w), 3742 (w), 3673 (w), 3649 (w), 3444 (w), 2937 (w), 1867 (w), 1672 (s), 1606 (m), 1541 (m), 1506 (m), 1456 (m), 1390 (s), 1296 (w), 1245 (m), 1199 (w), 1167 (m), 1095 (m), 1001 (w), 854 (s), 782 (m), 663 (s), 495 (s), 464 (s), 419 cm^{-1} (s).

Synthesis of DMOF-3 [Zn_5(me-btz)$_6$(L^1)(H_2O)]: The same synthetic conditions as those used for the preparation of **DMOF-2** were used except with **TMBB-3** instead of **TMBB-1**. The colorless block crystals were isolated by washing with DMF and were immersed in dichloromethane for 24 h. After the removal of dichloromethane by decanting, the sample was dried under a dynamic vacuum at room temperature overnight. Yield: 108.5 mg, 62 % based on H_4L^1. IR (KBr): $\tilde{\nu}$ = 3445 (m), 2929 (m), 1672 (s), 1601 (s), 1502 (m), 1386 (s), 1301 (m), 1246 (s), 1198 (s), 1168 (s), 1095 (s), 1057 (m), 1011 (m), 864 (w), 834 (w), 808 (w), 784 (m), 763 (w), 661 (m), 623 (w), 596 (w), 499 (w), 471 cm^{-1} (w).

Synthesis of DMOF-4 [Zn_5(btz)$_6$(L^2)(H_2O)$_2$]: A solid mixture of H_4L^2 (73.6 mg, 0.10 mmol) and **TMBB-1** (130.2 mg, 0.10 mmol) was dissolved in a mixture of DMF and 1-methyl-2-pyrrolidinone (NMP) (5.0/5.0 mL) in a 20 mL Teflon-lined stainless steel container. The clear reaction solution was heated in an isotherm oven at 85 °C for 72 h, resulting in colorless crystals, which were isolated by washing with DMF (5 × 5 mL) and were immersed in dichloromethane for 24 h. After the removal of dichloromethane by decanting, the sample was dried under a dynamic vacuum at room temperature overnight. Yield: 146.1 mg, 81 % based on 1 mol of H_4L^2. IR (KBr): $\tilde{\nu}$ = 3742 (w), 3443 (s), 2936 (m), 1672 (s), 1548 (m), 1507 (s), 1454 (s), 1389 (s), 1300 (s), 1265 (s), 1221 (m), 1112 (m), 1017 (w), 929 (w), 784 (m), 754 (m), 662 (w), 555 (w), 471 (w), 425 cm^{-1} (w).

Synthesis of DMOF-5 [Zn_5(bme-btz)$_6$(L^2)]: The same synthetic condition as that of **DMOF-4** was used except for **TMBB-2** instead of **TMBB-1**. The colorless block crystals were isolated by washing with DMF and were immersed in dichloromethane for 24 h. After the removal of dichloromethane by decanting, the sample was dried under a dynamic vacuum at room temperature overnight. Yield: 0153.0 mg, 79 % based on 1 mol of H_4L^2. IR (KBr): $\tilde{\nu}$ = 3429 (s), 2974 (m), 2500 (w), 1663 (s), 1596 (s), 1511 (s), 1461 (s), 1365 (s), 1281 (m), 1264 (s), 1112 (m), 1025 (m), 851 (w), 798 (m), 657 (w), 497 cm^{-1} (w).

Synthesis of DMOF-6 [Zn_5(me-btz)$_6$(L^2)]: The same synthetic conditions as those use for the preparation of **DMOF-4** were used except with **TMBB-3** instead of **TMBB-1**. The colorless block crystals were isolated by washing with DMF and were immersed in dichloromethane for 24 h. After the removal of dichloromethane by decanting, the sample was dried under a dynamic vacuum at room temperature overnight. Yield: 135.2 mg, 62 % based on 1 mol of H_4L^2. IR (KBr): $\tilde{\nu}$ = 3427 (m), 2933 (m), 1665 (s), 1600 (s), 1550 (m), 1509 (m), 1455 (s), 1415 (s), 1384 (s), 1266 (s), 1220 (s), 1110 (m), 1009 (m), 881 (w), 834 (w), 782 (m), 661 (m), 620 (w), 597 (w), 498 (w), 470 (w), 433 cm^{-1} (w).

Synthesis of DMOF-7: The same synthetic conditions as those used for the preparation of **DMOF-1** were used except with H_4L^3 instead of H_4L^1. The colorless microcrystals were isolated by washing with DMF and were immersed in dichloromethane for 24 h. After the removal of dichloromethane by decanting, the sample was dried under a dynamic vacuum at room temperature overnight. IR (KBr): $\tilde{\nu}$ = 3741 (w), 3443 (m), 3062 (m), 2930 (m), 1672 (s), 1627 (s), 1481 (s), 1382 (s), 1256 (s), 1209 (s), 1090 (m), 1026 (m), 866 (w), 783 (m), 750 (s), 650 (w), 553 (w), 474 cm^{-1} (w).

Synthesis of DMOF-8 [Zn_{15}(bme-btz)$_{18}$(L^3)$_3$ (H_2O)$_2$]: The same synthetic conditions as those used for the preparation of **DMOF-2** were used except with H_4L^3 instead of H_4L^1 and *N,N*-diethylformamide (DEF) instead of DMF. The colorless block crystals were isolated by washing with DMF and were immersed in dichloromethane for 24 h. After the removal of dichloromethane by decanting, the sample was dried under a dynamic vacuum at room temperature overnight. Yield: 142.4 mg, 69 % based on 1 mol of H_4L^3. IR (KBr): $\tilde{\nu}$ = 3924 (w), 3859 (w), 3742 (m), 3673 (w), 3649 (w), 3591 (m), 3564 (m), 3445 (m), 2976 (s), 2939 (m), 2884 (m), 1671 (s), 1541 (s), 1514 (m), 1456 (s), 1395 (s), 1297 (w), 1262 (m), 1212 (s), 1109 (m), 1025 (w), 944 (w), 856 (w), 824 (w), 765 (w), 672 (w), 644 (w), 495 (m), 418 cm^{-1} (s).

Synthesis of DMOF-9 [Zn_5(btz)$_6$(L^4)]: The same synthetic conditions as those used for the preparation of **DMOF-1** were used except with H_4L^4 instead of H_4L^1. The colorless block crystals were isolated by washing with DMF and were immersed in dichloromethane for 24 h. After the removal of dichloromethane by decanting, the sample was dried under a dynamic vacuum at room temperature overnight. Yield: 147.2 mg, 84 % based on 1 mol of H_4L^4. IR (KBr): $\tilde{\nu}$ = 3438 (s), 2940 (m), 2882 (m), 1664 (s), 1604 (s), 1508 (s), 1390 (s), 1300 (m), 1236 (s), 1173 (s), 1099 (m), 1031 (w), 987 (w), 834 (w), 782 (w), 750 (m), 643 (w), 555 cm^{-1} (m).

Synthesis of DMOF-10: The same synthetic conditions as those used for the preparation of **DMOF-2** were used except with H_4L^4 instead of H_4L^1. The colorless microcrystals were isolated by washing with DMF and were immersed in dichloromethane for 24 h. After the removal of dichloromethane by decanting, the sample was dried under a dynamic vacuum at room temperature overnight. IR (KBr): $\tilde{\nu}$ = 3438 (m), 2975 (s), 2938 (w), 1671 (s), 1602 (s), 1510 (m), 1429 (s), 1391 (s), 1303 (m), 1237 (s), 1171 (s), 1109 (m), 1003 (w), 826 (m), 785 (w), 747 (w), 641 (w), 497 (m), 465 cm^{-1} (w).

Synthesis of DMOF-11 [Zn_5(me-btz)$_6$(L^4)]: The same synthetic conditions as those used for the preparation of **DMOF-3** were used except with H_4L^4 instead of H_4L^1. The colorless block crystals were isolated by washing with DMF and were immersed in dichloromethane for 24 h. After the removal of dichloromethane by decanting, the sample was dried under a dynamic vacuum at room temperature overnight. Yield: 145.0 mg, 79 % based on 1 mol of H_4L^4. IR (KBr): $\tilde{\nu}$ = 3438 (m), 2970 (s), 2940 (w), 1671 (s), 1603 (s), 1510 (m), 1430 (s), 1391 (s), 1303 (m), 1237 (s), 1171 (s), 1109 (m), 1033 (w), 826 (m), 785 (w), 749 (w), 641 (w), 497 cm^{-1} (m).

Synthesis of DMOF-12: The same synthetic conditions as those used for the preparation of **DMOF-4** were used except with H_4L^5 instead of H_4L^2. The colorless microcrystals were isolated by washing with DMF and were immersed in dichloromethane for 24 h. After the removal of dichloromethane by decanting, the sample was dried under a dynamic vacuum at room temperature overnight. IR (KBr): $\tilde{\nu}$ = 3436 (m), 2935 (m), 1670 (s), 1595 (s), 1510 (s), 1448 (s), 1386 (s), 1264 (s), 1201 (s), 1134 (m), 1091 (m), 1026 (m), 850 (w), 814 (w), 783 (w), 751 (m), 719 (w), 642 (w), 555 cm^{-1} (w).

Synthesis of DMOF-13 [Zn_5(btz)$_6$(L^6)(H_2O)]: The same synthetic conditions as those used for the preparation of **DMOF-4** were used except with H_4L^6 instead of H_4L^2. The colorless block crystals were isolated by washing with DMF and were immersed in dichloromethane for 24 h. After the removal of dichloromethane by decanting, the sample was dried under a dynamic vacuum at room temperature overnight. Yield: 167.5 mg, 85 % based on 1 mol of H_4L^6. IR (KBr): $\tilde{\nu}$ = 3447 (m), 2931 (m), 1672 (s), 1602 (s), 1504 (m), 1390 (s), 1299 (m), 1240 (s), 1174 (s), 1095 (s), 1017 (w), 864 (w), 785 (s), 740 (m), 662 (m), 594 (w), 474 cm^{-1} (w).

Synthesis of DMOF-14: The same synthetic conditions as those used for the preparation of **DMOF-5** were used except with H_4L^6 instead of H_4L^2. The colorless block crystals were isolated by washing with DMF and were immersed in dichloromethane for 24 h. After the removal of dichloromethane by decanting, the sample was dried under a dynamic vacuum at room temperature overnight. IR (KBr): $\tilde{\nu}$ = 3443 (s), 2933 (w), 1672 (s), 1502 (s), 1390 (s), 1299 (s), 1258 (s), 1174 (m), 1095 (m), 853 (w), 783 (w), 659 (m), 469 cm^{-1} (s).

Synthesis of DMOF-15: The same synthetic conditions as those used for the preparation of **DMOF-6** were used except with H_4L^6 instead of H_4L^2. The colorless microcrystals were isolated by washing with DMF and were immersed in dichloromethane for 24 h. After the removal of dichloromethane by decanting, the sample was dried under a dynamic vacuum at

room temperature overnight. IR (KBr): $\tilde{\nu}$ = 3419 (m), 2935 (w), 1634 (s), 1497 (s), 1398 (s), 1267 (s), 1240 (s), 1187 (s), 1012 (s), 863 (w), 834 (m), 808 (w), 784 (m), 740 (w), 594 (m), 474 cm^{-1} (m).

X-ray crystallography: Single-crystal X-ray data of **TMBB-1**, **TMBB-2**, and **DMOF-1**, **2**, **3**, **4**, **5**, **6**, **8**, **9**, **11**, **13**, and **MOF-01** were recorded by using a Bruker Apex CCD diffractometer with graphite-monochromated $Mo_{K\alpha}$ radiation (λ = 0.71073 Å) at T = 293 K. Absorption corrections were applied by using a multiscan technique. All the structures were solved by the direct method of SHELXS-97 and refined by full-matrix least-squares techniques using the SHELXL-97 program within WINGX. The solvent molecules are highly disordered, and attempts to locate and refine the solvent peaks were unsuccessful. Contributions to scattering due to these solvent molecules were removed using the SQUEEZE routine of PLATON; structures were then refined again using the data generated. Crystal data are summarized in Table S1 in the Supporting Information. CCDC-854810 (**TMBB-1**), CCDC-854811 (**TMBB-2**), CCDC-854812 (**DMOF-1**), CCDC-854813 (**DMOF-2**), CCDC-854814 (**DMOF-3**), CCDC-854815 (**DMOF-4**), CCDC-854816 (**DMOF-5**), CCDC-854817 (**DMOF-6**), CCDC-854818 (**DMOF-8**), CCDC-854819 (**DMOF-9**), CCDC-854820 (**DMOF-11**), CCDC-854821 (**DMOF-13**) and CCDC-854822 (**MOF-01**) contain the supplementary crystallographic data for this paper. These data can be obtained free of charge from The Cambridge Crystallographic Data Centre via www.ccdc.cam.ac.uk/data_request/cif.

Acknowledgements

We gratefully thank the AIST and JSPS for financial support. Y.Q.L. thanks the JSPS for a postdoctoral fellowship.

[1] a) M. Eddaoudi, J. Kim, N. Rosi, D. Vodak, J. Wachter, M. O'Keeffe, O. M. Yaghi, *Science* **2002**, *295*, 469–472; b) G. Férey, C. Mellot-Draznieks, C. Serre, F. Millange, *Acc. Chem. Res.* **2005**, *38*, 217–225; c) S. Kitagawa, R. Kitaura, S. Noro, *Angew. Chem.* **2004**, *116*, 2388–2430; *Angew. Chem. Int. Ed.* **2004**, *43*, 2334–2375; d) K. Otsubo, Y. Wakabayashi, J. Ohara, S. Yamamoto, H. Matsuzaki, H. Okamoto, K. Nitta, T. Uruga, H. Kitagawa, *Nat. Mater.* **2011**, *10*, 291–295; e) J. R. Li, H.-C. Zhou, *Nat. Chem.* **2010**, *2*, 893–898; f) D. J. Lun, G. I. N. Waterhouse, S. G. Telfer, *J. Am. Chem. Soc.* **2011**, *133*, 5806–5809.

[2] a) J. S. Seo, D. Whang, H. Lee, S. I. Jun, J. Oh, Y. J. Jeon, K. Kim, *Nature* **2000**, *404*, 982–986; b) L. Pan, D. H. Olson, L. R. Ciemnolonski, R. Heddy, J. Li, *Angew. Chem.* **2006**, *118*, 632–635; *Angew. Chem. Int. Ed.* **2006**, *45*, 616–619; c) A. M. Shultz, O. K. Farha, J. T. Hupp, S. T. Nguyen, *J. Am. Chem. Soc.* **2009**, *131*, 4204–4205; d) Y. E. Cheon, M. P. Suh, *Angew. Chem.* **2009**, *121*, 2943–2947; *Angew. Chem. Int. Ed.* **2009**, *48*, 2899–2903; e) H. L. Jiang, Q. Xu, *Chem. Commun.* **2011**, *47*, 3351–3370; f) H. Kitagawa, *Nat. Chem.* **2009**, *1*, 689–690; g) B. Chen, S. Xiang, G. Qian, *Acc. Chem. Res.* **2010**, *43*, 1115–1124; h) R. E. Morris, X. Bu, *Nat. Chem.* **2010**, *2*, 353–361; i) S.-T. Zheng, J. T. Bu, Y. Li, T. Wu, F. Zuo, P. Feng, X. Bu, *J. Am. Chem. Soc.* **2010**, *132*, 17062–17064; j) B. Zheng, J. Bai, J. Duan, L. Wojtas, M. J. Zaworotko, *J. Am. Chem. Soc.* **2011**, *133*, 748–751; k) G. Xu, X. Zhang, P. Guo, C. Pan, H. Zhang, C. Wang, *J. Am. Chem. Soc.* **2010**, *132*, 3656–3657.

[3] a) B. J. Burnett, P. M. Barron, C. Hu, W. Choe, *J. Am. Chem. Soc.* **2011**, *133*, 9984–9987; b) Z. Zhang, S. Xiang, Y. S. Chen, S. Ma, Y. Lee, T. Phely-Bobin, B. Chen, *Inorg. Chem.* **2010**, *49*, 8444–8448.

[4] Y. L. Bai, J. Tao, R.-B. Huang, L.-S. Zheng, *Angew. Chem.* **2008**, *120*, 5424–5427; *Angew. Chem. Int. Ed.* **2008**, *47*, 5344–5347.

[5] J. D. Wuest, *Chem. Commun.* **2005**, 5830–5837.

[6] a) M. W. Hosseini, *CrystEngComm* **2004**, *6*, 318–322; b) M. W. Hosseini, *Acc. Chem. Res.* **2005**, *38*, 313–323.

[7] a) M. Eddaoudi, D. B. Moler, H. Li, B. Chen, T. M. Reineke, M. O'Keeffe, O. M. Yaghi, *Acc. Chem. Res.* **2001**, *34*, 319–330; b) O. M. Yaghi, M. O'Keeffe, N. W. Ockwig, H. K. Chae, M. Eddaoudi, J. Kim, *Nature* **2003**, *423*, 705–714.

[8] a) X. L. Wang, C. Qin, S. X. Wu, K. Z. Shao, Y. Q. Lan, S. Wang, D. X. Zhu, Z. M. Su, E. B. Wang, *Angew. Chem.* **2009**, *121*, 5395–5399; *Angew. Chem. Int. Ed.* **2009**, *48*, 5291–5295; b) J. R. Li, D. J. Timmons, H. C. Zhou, *J. Am. Chem. Soc.* **2009**, *131*, 6368–6369; c) A. Schoedel, L. Wojtas, S. P. Kelley, R. D. Rogers, M. Eddaoudi, M. J. Zaworotko, *Angew. Chem.* **2011**, *123*, 11623–11626; *Angew. Chem. Int. Ed.* **2011**, *50*, 11421–11424; d) H. N. Wang, X. Meng, G. S. Yang, X. L. Wang, K. Z. Shao, Z. M. Su, C. G. Wang, *Chem. Commun.* **2011**, *47*, 7128–7130.

[9] a) Z. Wang, S. M. Cohen, *Chem. Soc. Rev.* **2009**, *38*, 1315–1329; b) K. K. Tanabe, S. M. Cohen, *Chem. Soc. Rev.* **2011**, *40*, 498–519; c) S. M. Cohen, *Chem. Sci.* **2010**, *1*, 32–36; d) Y.-F. Song, L. Cronin, *Angew. Chem.* **2008**, *120*, 4713–4715; *Angew. Chem. Int. Ed.* **2008**, *47*, 4635–4637; e) S. M. Cohen, *Chem. Rev.* **2012**, *112*, 970–1000.

[10] B. F. Hoskins, R. Robson, *J. Am. Chem. Soc.* **1990**, *112*, 1546–1554.

[11] Y.-H. Kiang, G. B. Gardner, S. Lee, Z. Xu, E. Lobkovsky, *J. Am. Chem. Soc.* **1999**, *121*, 8204–8205.

[12] M. J. Zaworotko, *Nat. Chem.* **2009**, *1*, 267–268.

[13] S. R. Batten, R. Robson, *Angew. Chem.* **1998**, *110*, 1558–1595; *Angew. Chem. Int. Ed.* **1998**, *37*, 1460–1494.

[14] A. J. Blake, N. R. Champness, S. S. M. Chung, W. S. Li, M. Schröder, *Chem. Commun.* **1997**, 1005–1006.

[15] Y.-Q. Lan, H.-L. Jiang, S.-L. Li, Q. Xu, *Adv. Mater.* **2011**, *23*, 5015–5020.

[16] X.-J. Luan, Y.-Y. Wang, D.-S. Li, P. Liu, H.-M. Hu, Q.-Z. Shi, S.-M. Peng, *Angew. Chem.* **2005**, *117*, 3932–3935; *Angew. Chem. Int. Ed.* **2005**, *44*, 3864–3867.

[17] A. L. Spek, *J. Appl. Crystallogr.* **2003**, *36*, 7–13.

[18] J. T. Jia, F. X. Sun, Q. R. Fang, X. Q. Liang, K. Cai, Z. Bian, H. J. Zhao, L. X. Gao, G. S. Zhu, *Chem. Commun.* **2011**, *47*, 9167–9169.

[19] J. Sculley, D. Yuan, H.-C. Zhou, *Energy Environ. Sci.* **2011**, *4*, 2721–2735.

[20] H. Deng, C. J. Doonan, H. Furukawa, R. B. Ferreira, J. Towne, C. B. Knobler, B. Wang, O. M. Yaghi, *Science* **2010**, *327*, 846–850.

Received: March 2, 2012
Published online: May 22, 2012

